Multiscale Model. Simul.
Vol. 13, No. 1, pp. 440–458

DIFFRACTONS: SOLITARY WAVES CREATED BY DIFFRACTION IN PERIODIC MEDIA*

DAVID I. KETCHESON† AND MANUEL QUEZADA DE LUNA‡

Abstract. A new class of solitary waves arises in the solution of nonlinear wave equations with constant impedance and no dispersive terms. These solitary waves depend on a balance between nonlinearity and a dispersion-like effect due to spatial variation in the sound speed of the medium. A high-order homogenized model confirms this effective dispersive behavior, and its solutions agree well with those obtained by direct simulation of the variable-coefficient system. These waves are observed to be long-time stable, globally attracting solutions that arise in general as solutions to nonlinear wave problems with periodically varying sound speed. They share some properties with known classes of solitary waves but possess important differences as well.

Key words. solitary waves, periodic media, diffraction, homogenization

AMS subject classifications. 35L50, 35B27, 37K40

DOI. 10.1137/130946526

1. Introduction.

Many nonlinear wave equations are known to have solitary wave (or soliton) solutions. These partial differential equations, such as the Korteweg–de Vries or nonlinear Schrödinger equation, include both nonlinear and dispersive terms. Solitary wave solutions arise through a balance between nonlinear and dispersive effects.

Solitary wave solutions have also been observed—in the absence of dispersive terms—in simulations of periodic elastic media with spatially varying impedance [10, 6, 7, 12]. Such media exhibit an effective dispersion—the result of reflections due to the material structure. This effective dispersion is present only in media with spatially varying impedance; waves in one-dimensional media with uniform impedance behave, at the macroscopic scale, essentially like waves in a homogeneous medium [14, 10, 7].

Herein we report the discovery of solitary wave solutions to a first-order hyperbolic system with *no dispersive terms* and *no reflection*. These solitary waves arise in two-dimensional periodic media in which *the impedance is constant* and only the sound speed varies. The mechanism responsible for the effective dispersion that leads to these waves is diffraction [13]. We thus refer to these waves as *diffractons*. Computational evidence suggests that diffractons are globally attracting solutions to quite general classes of nonlinear wave equations in periodic materials.

In this work, we investigate diffractons through computation and analysis. The paper is organized as follows. In section 2, we present the model, materials, and waves that are the subject of this study. In section 3 we derive an effective model for two-dimensional (2D) nonlinear waves in periodic media based on homogenization. In section 4 we study symmetries and interactions of diffractons. Finally, in section

*Received by the editors November 25, 2013; accepted for publication (in revised form) October 21, 2014; published electronically March 31, 2015. This research was supported by The King Abdullah University of Science and Technology (KAUST).

http://www.siam.org/journals/mms/13-1/94652.html

†Division of Computer, Electrical and Mathematical Sciences, 4700 King Abdullah University of Science and Technology (KAUST), Thuwal, 23955-6900, Kingdom of Saudi Arabia (david.ketcheson@kaust.edu.sa).

‡Department of Mathematics, Texas A&M University, College Station, TX 77843 (mquezada@math.tamu.edu).

5, we show that diffractons arise in a wide range of settings.

2. Solitary waves in nondispersive, constant-impedance, periodic media. We are interested in the behavior of multidimensional waves in nonlinear, spatially varying media. Essentially, the simplest model of this kind is

$$\epsilon_{tt} - \nabla \cdot \left(\frac{1}{\rho(\mathbf{x})} \nabla \sigma(\epsilon, \mathbf{x}) \right) = 0, \tag{1}$$

which may be viewed as a multidimensional analogue of the p-system. We use the notation of elasticity for consistency with related work [10, 12]; thus ϵ is the strain, ρ is the density, and σ is the stress. If the stress-strain function is linear, i.e., $\sigma(\epsilon, \mathbf{x}) = K(\mathbf{x})\epsilon$, then (1) is just the variable-coefficient linear wave equation.

If the stress-strain relation is nonlinear, then solutions of (1) often involve shock singularities. In most of what follows, we take

$$\sigma(\epsilon, \mathbf{x}) = \exp(K(\mathbf{x})\epsilon) - 1. \tag{2}$$

Here $K(\mathbf{x})$ is referred to as the bulk modulus. The particular relation (2) is convenient for performing homogenization, but the phenomenon under study seems to appear when σ is any nonlinear function.

Solutions of (1) with the stress relation (2) often involve shock singularities. In order to determine entropy-satisfying weak solutions, we write (1) as a first-order hyperbolic system of conservation laws:

$$\mathbf{q}_t + \mathbf{f}(\mathbf{q}, \mathbf{x})_x + \mathbf{g}(\mathbf{q}, \mathbf{x})_y = \mathbf{0}, \tag{3a}$$

where

$$\mathbf{q} = \begin{bmatrix} \epsilon \\ \rho(\mathbf{x})u \\ \rho(\mathbf{x})v \end{bmatrix}, \qquad \mathbf{f}(\mathbf{q}, \mathbf{x}) = \begin{bmatrix} -u \\ -\sigma(\epsilon, \mathbf{x}) \\ 0 \end{bmatrix}, \qquad \mathbf{g}(\mathbf{q}, \mathbf{x}) = \begin{bmatrix} -v \\ 0 \\ -\sigma(\epsilon, \mathbf{x}) \end{bmatrix}. \tag{3b}$$

Here u and v are the x- and y-components of velocity, $\mathbf{q}$ is the vector of conserved quantities, and $\mathbf{f}, \mathbf{g}$ are the components of the flux in the x- and y-directions, respectively.

We consider media in which the material parameters are uniform in one direction (x) and vary periodically in the other (y) with period Ω; i.e., $K = K(y)$, $\rho = \rho(y)$ with

$$K(y + \Omega) = K(y), \qquad \rho(y + \Omega) = \rho(y).$$

We take $\Omega = 1$ throughout this work. The linearized sound speed $c(y) = \sqrt{K/\rho}$ and linearized impedance $Z(y) = \sqrt{K\rho}$ are thus also periodic and will play a central role in our analysis.

We primarily investigate piecewise-constant (layered) media, as shown in Figure 1:

$$K(y), \rho(y) = \begin{cases} (K_A, \rho_A) & \text{if } \left(y - \lfloor y \rfloor - \frac{1}{2}\right) < 0, \\ (K_B, \rho_B) & \text{if } \left(y - \lfloor y \rfloor - \frac{1}{2}\right) > 0. \end{cases} \tag{4}$$

We use the terms *normal wave* and *transverse wave* to indicate plane wave perturbations traveling orthogonal to or parallel to the layer interfaces, as indicated in Figure

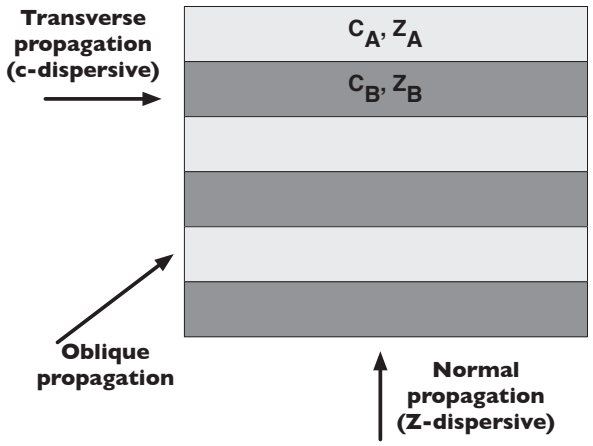

FIG. 1. *2D wave propagation in a one-dimensionally periodic medium. A piecewise-constant layered medium is shown. We take* $\Omega = 1$ *throughout this work.*

1. Note that these terms, as used herein, have nothing to do with the distinction between compression and shear waves; our model supports only compression waves. Propagation of a normally incident plane wave can (by symmetry) be modeled as a one-dimensional problem; in this case our model reduces to that studied in [10]. There it was observed that solitary waves can form when the impedance contrast is sufficiently high, due to the net effect of reflections. When the impedance is uniform, normal waves behave similarly to solutions of Burgers' equation, leading to shock formation and N-wave decay [7].

In the present work, we are mainly interested in transversely-propagating waves, i.e., those arising from perturbations that are uniform in y. As we will see, such perturbations can lead to solitary wave formation even when the impedance is constant. The effect responsible for this is diffraction, which appears whenever the medium sound speed varies. Note that, unlike normal perturbations, transverse perturbations represent a genuinely 2D phenomenon.

Let us conduct a few computational experiments to indicate the types of behavior possible for transversely-propagating waves. We consider a wave entering the domain from the left generated by a moving wall boundary condition:

$$\rho(y)u(0,y,t) = \begin{cases} 0.1(1+\cos(\pi(t-10)/10)), & 0 \le t \le 20, \\ 0, & t \ge 20. \end{cases} \tag{5}$$

By symmetry, the problem can be solved by considering a single period of the medium and periodic boundary conditions in y. We compute solutions to (1) using the finite volume solver PyClaw [8, 16] with the Riemann solvers described in [12]. We consider the solution after the perturbation has traveled a distance of more than 300 material periods.

First we consider the simpler case of linear wave propagation by taking the linear constitutive relation

$$\sigma(\epsilon, \mathbf{x}) = K(y)\epsilon$$

in place of (2). It turns out that the resulting solution depends qualitatively on whether the sound speeds in the two materials are equal or not. Figure 2(a) (note the

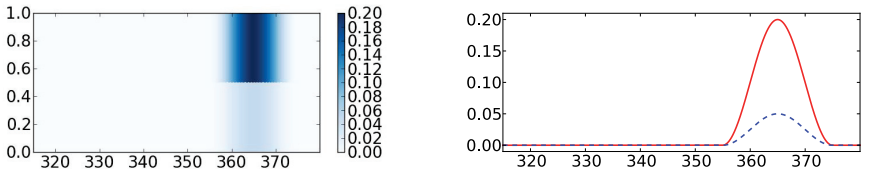

(a) Linear medium, constant c

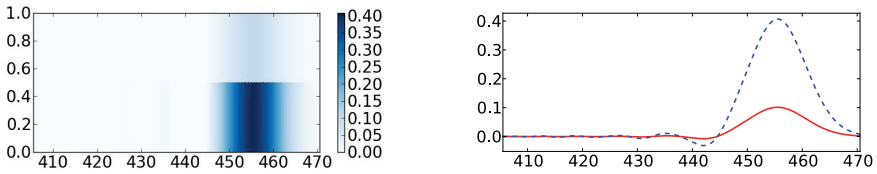

(b) Linear medium, variable c

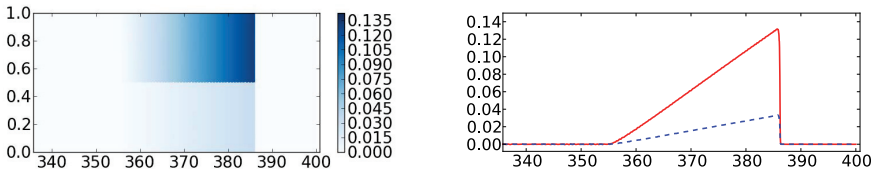

(c) Nonlinear medium, constant c

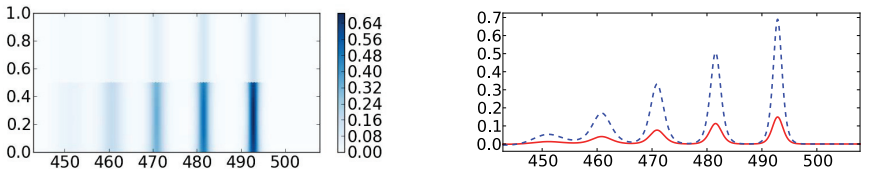

(d) Nonlinear medium, variable c

FIG. 2. *Strain at $t = 375$ for four experiments. We show surface plots (left; note high aspect ratio) and y-slices (right) at the middle of material A ($y = 0.25$; blue) and material B ($y = 0.75$; red).*

very high aspect ratio) shows the solution obtained in a medium with parameters

$$c_A = 1, \qquad Z_A = 4, \tag{6a}$$

$$c_B = 1, \qquad Z_B = 1, \tag{6b}$$

obtained by taking $K_A = \rho_A = 4$ and $K_B = \rho_B = 1$. Because $c_A = c_B$, the initial perturbation travels at constant velocity without changing shape.

Figure 2(b) shows a solution obtained with

$$c_A = 5/8, \qquad Z_A = 1, \tag{7a}$$

$$c_B = 5/2, \qquad Z_B = 1, \tag{7b}$$

obtained by taking $K_A = 1/\rho_A = 5/8$ and $K_B = 1/\rho_B = 5/2$. Since $c_A \neq c_B$, the initial perturbation undergoes diffraction, leading to an effective dispersion. High frequencies travel more slowly, so the solution develops an oscillatory tail. We emphasize that this *effective dispersion* is a macroscopic effect of the material microstructure; clearly, no dispersive terms appear in the model equations. This effect has been studied in detail for linear waves in [13].

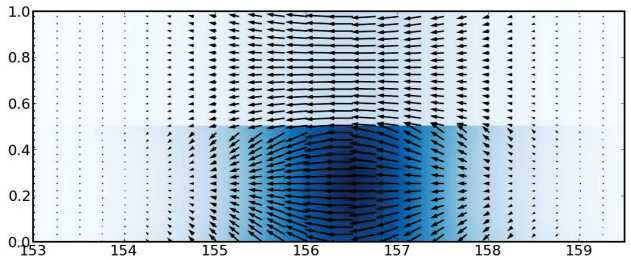

FIG. 3. *Structure of a diffracton. Strain is shown in blue, and vectors represent the material velocity. The solitary wave travels only to the right, but diffraction is evident in the (vertical) material velocities.*

Next we consider the same two scenarios, but with the nonlinear stress relation (2). Figure 2(c) shows the solution for a medium with linearized sound speed and impedance given by (6), so that $c_A = c_B = 1$. The solution behaves like a one-dimensional perturbation in a homogeneous medium. A shock forms and leads to gradual decay of the solution amplitude.

Finally, in Figure 2(d), we consider the main case of interest: a nonlinear medium with linearized sound speed and impedance given by (7), so that $c_A \neq c_B$. The combination of nonlinearity and effective (diffractive) dispersion leads to the formation of a train of solitary waves. We refer to these waves as *diffractons*. A typical diffracton is shown in Figure 3. Notice that, although this solitary wave simply translates to the right, vertical velocities appear in the solution due to diffraction.

3. Homogenization. Analysis of the wave equation (1) is complicated by the presence of variable coefficients. Here we derive a homogenized approximation with constant coefficients and use it to investigate diffractons.

In [13], high-order homogenized equations are derived for *linear* acoustic waves in a medium of the type considered in this work. It is assumed that λ, the typical wavelength of the solution, is large compared to Ω, the period of the medium, so that $\delta = \Omega/\lambda$ is a small parameter. Here we apply the same homogenization process to the nonlinear system (3) to derive homogenized equations with $\mathcal{O}(\delta^2)$ corrections. Details of the homogenization process are deferred to Appendix B. The resulting homogenized system is

$$\begin{aligned} K_h^{-1}\sigma_t - (\sigma+1)(u_x+v_y) &= \delta^2\alpha_1\left[(\sigma+1)(u_{xyy}+v_{yyy}) + 2\sigma_y(u_{xy}+v_{yy})\right] \\ &\quad + \delta^2\alpha_2\left[(\sigma+1)(u_{xxx}+v_{xxy}) + 2\sigma_x(u_{xx}+v_{xy})\right] \\ &\quad + \delta^2\alpha_3\sigma_y(u_{xy}+v_{yy}), \qquad \text{(8a)} \\ \rho_h u_t - \sigma_x &= \delta^2\beta_1\sigma_{xyy} + \delta^2\beta_2\sigma_{xxx}, \qquad \text{(8b)} \\ \rho_m v_t - \sigma_y &= \delta^2\gamma_1\sigma_{yyy} + \delta^2\gamma_2\sigma_{xxy}, \qquad \text{(8c)} \end{aligned}$$

where the values of the coefficients α, β, γ depend on the the material coefficient functions $K(y), \rho(y)$. The subscripts m and h denote the arithmetic and harmonic average, respectively; for instance,

$$\rho_m = \int_0^1 \rho(y)dy, \qquad \rho_h = \left(\int_0^1 \frac{1}{\rho(y)}dy\right)^{-1}.$$

Observe that the $\mathcal{O}(1)$ terms in (8) represent a straightforward averaging of the variable-coefficient equations. Meanwhile, the $\mathcal{O}(\delta^2)$ terms introduce dispersion. For the layered medium (4), it is possible to obtain closed-form expressions for the dispersive term coefficients:

$$\gamma_1 = \lambda^2 \left(Z_A^2 - Z_B^2\right) \frac{(\rho_A - \rho_B)}{192 K_m \rho_m^2}, \qquad \gamma_2 = \lambda^2 \left(c_A^2 - c_B^2\right) \frac{(\rho_A - \rho_B)}{192 K_m}, \tag{9a}$$

$$\beta_1 = \lambda^2 \left(Z_A^2 - Z_B^2\right) \frac{(\rho_B - \rho_A)}{192 K_m \rho_m^2}, \qquad \beta_2 = \lambda^2 \left(c_A^2 - c_B^2\right) \frac{(\rho_B - \rho_A)}{192 K_m}, \tag{9b}$$

$$\alpha_1 = \lambda^2 \left(Z_A^2 - Z_B^2\right) \frac{(K_A - K_B)}{192 K_m^2 \rho_m}, \qquad \alpha_2 = \lambda^2 \left(c_A^2 - c_B^2\right) \frac{(K_A - K_B)\,\rho_m}{192 K_m^2}, \tag{9c}$$

$$\alpha_3 = \lambda^2 \frac{(\rho_A - \rho_B)^2}{192 \rho_m^2}. \tag{9d}$$

Notice that $\alpha_1, \beta_1, \gamma_1$ vanish when $Z_A = Z_B$, whereas $\alpha_2, \beta_2, \gamma_2$ vanish when $c_A = c_B$. These properties will play an important role in what follows.

3.1. Normally-propagating plane waves. For initial data that do not vary in x, solutions to (8) are plane waves traveling in the normal direction (parallel to the y-axis). For such waves, system (8) simplifies to

$$K_h^{-1}\sigma_t - (\sigma + 1)\, v_y = \delta^2 \alpha_1 (\sigma + 1)\, v_{yyy} + \delta^2 (\alpha_3 + 2\alpha_1)\, \sigma_y v_{yy}, \tag{10a}$$

$$\rho_m v_t - \sigma_y = \delta^2 \gamma_1 \sigma_{yyy}. \tag{10b}$$

The corresponding one-dimensional problem is studied extensively in [10], and (10) is equivalent (up to $\mathcal{O}(\delta^2)$) to the approximation derived there. This homogenized system (and the original variable-coefficient equation) possesses solitary wave solutions, due to the combination of nonlinearity and an effective dispersion that arises due to reflection. We do not pursue this case further here except to observe that most of the dispersive terms vanish when the linearized impedance is constant (i.e., when there is no reflection).

3.2. Transversely-propagating plane waves. For initial data that do not vary in y, solutions to (8) are plane waves traveling in the transverse direction (parallel to the x-axis). For such waves, system (8) simplifies to

$$K_h^{-1}\sigma_t - (\sigma + 1)\, u_x = \delta^2 \alpha_2 \left[(\sigma + 1)\, u_{xxx} + 2\sigma_x u_{xx}\right], \tag{11a}$$

$$\rho_h u_t - \sigma_x = \delta^2 \beta_2 \sigma_{xxx}. \tag{11b}$$

As our introductory experiments (see Figure 2) suggest, this system possesses solitary wave solutions as long as the sound speed is not constant. On the other hand, if the linearized sound speed is constant, then all the dispersive term coefficients vanish. This is because the effective dispersive mechanism in this case is that of diffraction, which occurs only if the sound speeds differ [13]. In the absence of diffraction, nonlinearity leads to shock formation, as observed in Figure 2(c).

In Figure 4, we compare the numerical solution of (11) with that of the variable coefficient 2D wave equation (1) arithmetically averaged in y. The initial condition is

$$\sigma_0(x, y) = e^{-x^2/10}, \qquad u_0 = v_0 = 0. \tag{12}$$

The solitary wave solutions of (11) are a reasonably good approximation of the solutions of (1) and could be improved by including higher-order terms.

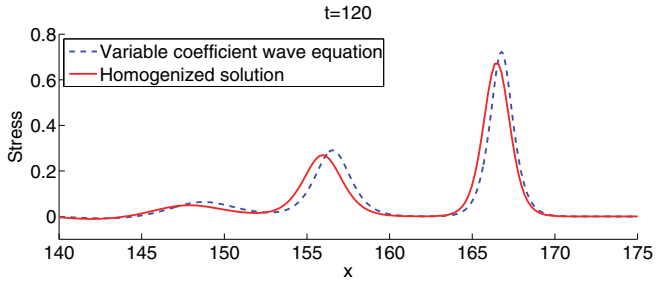

FIG. 4. *Solution of one-dimensional homogenized equations* (11) *(solid red) versus y-averaged solution of the two-dimensional variable-coefficient wave equation* (1) *(dashed blue).*

3.3. Stationary solutions of the homogenized equations. In this section, we assume a traveling wave solution for (11) and derive an ODE for the shape of a homogenized $\mathcal{O}(\delta^2)$ diffracton. Afterward, following section 10 of [6], we use this ODE to find a lower limit for the speed of a diffracton.

Consider system (11) and assume a traveling wave solution of the form $\sigma + 1 = W(x - Vt)$ and $u = U(x - Vt)$, where V is the speed of the traveling wave. After combining the resulting equations and dropping terms of $\mathcal{O}(\delta^4)$, we get

$$W' = \frac{1}{M^2}\left[WW' + \delta^2(\alpha_2 + \beta_2)WW''' + 2\alpha_2\delta^2 W'W''\right]. \tag{13}$$

Here we have introduced the Mach number $M = V/c_{\text{eff}}$, where $c_{\text{eff}} = \sqrt{K_h/\rho_m}$ is the speed at which small-amplitude, long-wavelength perturbations travel in the transverse direction. For the layered medium (4), the coefficients α_2 and β_2 are given by (9), and their sum is nonnegative:

$$\alpha_2 + \beta_2 = \lambda^2 \frac{(c_A^2 - c_B^2)^2}{192K_m^2/(\rho_m\rho_h)} \geq 0. \tag{14}$$

Numerically integrating (13) with an appropriate velocity V yields solitary waves nearly identical to the homogenized diffractons of Figure 4.

Larger-amplitude waves move faster than c_{eff}, while short-wavelength, small-amplitude waves move more slowly (due to diffractive dispersion). Since diffractons are nonlinear waves with wavelength on the order of a few material layers, it is not clear a priori whether their speed should be larger or smaller than c_{eff}. Here we show that the homogenized equations dictate that diffractons move faster than c_{eff}; this is confirmed experimentally in section 4.2.

Integrate (13) by parts, and let $w_1 = W$ and $w_2 = W'$ to get

$$w_1' = w_2, \tag{15a}$$

$$w_2' = -\frac{(\alpha_2 - \beta_2)w_2^2}{(\alpha_2 + \beta_2)w_1} - \frac{w_1}{2\delta^2(\alpha_2 + \beta_2)} + \frac{M^2}{\delta^2(\alpha_2 + \beta_2)}\left(1 - \frac{2 - M^{-2}}{2w_1}\right). \tag{15b}$$

The equilibrium points are $(1, 0)$ and $(2M^2 - 1, 0)$, and the Jacobian is

$$J = \begin{bmatrix} 0 & 1 \\ -\frac{1-2M^2+w_1^2-2(\alpha_2-\beta_2)\delta^2 w_2^2}{2(\alpha_2+\beta_2)\delta^2 w_1^2} & \frac{-2(\alpha_2-\beta_2)w_2}{(\alpha_2+\beta_2)w_1} \end{bmatrix}, \tag{16}$$

whose eigenvalues at $(1,0)$ and $(2M^2-1,0)$ are

$$\lambda_l = \pm\frac{\sqrt{M^2-1}}{\delta\sqrt{\alpha_2+\beta_2}}, \qquad \lambda_r = \pm\frac{\sqrt{1-M^2}}{\delta\sqrt{(\alpha_2+\beta_2)(2M^2-1)}}, \tag{17}$$

respectively. The boundary conditions for a solitary wave are $W \to 1$ and $W', W'', W''' \to 0$ as $|x-Vt| \to \infty$, corresponding to the equilibrium point $(1,0)$; thus, diffractons correspond to homoclinic connections for this point. A homoclinic connection occurs if the equilibrium point $(1,0)$ is a saddle and $(2M^2-1,0)$ is a center. This happens only when $|M|>1$, so the homogenized diffractons are "supersonic." This property also holds for stegotons [6].

4. Properties and dynamics of diffractons. In this section we investigate the properties of diffractons: their stability, shape, scaling properties, speed-amplitude relation, and interactions.

4.1. Long-time stability. We have already seen that numerical solutions of both (1) and (8) may lead to the appearance of diffractons from general initial data. Indeed, it seems that diffractons are globally attracting solutions. To further investigate their long-time behavior we take a single diffracton from the solution of (1) as initial data and propagate it to $t=600$; the diffracton travels more than 600 units in space. Let $X(t)$ denote the grid location of the diffracton peak at time t. We compute the maximum relative difference between the solution at $t=0$ and the (recentered) solution at time t:

$$D = \max_t \left(\frac{\|\sigma(x-X(0),y,t=0) - \sigma(x-X(t),y,t)\|_{2(x,y)}}{\|\sigma(x-X(0),y,t=0)\|_{2(x,y)}} \right). \tag{18}$$

We consider two different grids: on a grid with $\Delta x = \Delta y = 1/16$ the maximum difference is $D = 4.6\%$; with $\Delta x = \Delta y = 1/32$, it is $D = 2.2\%$. Because we have taken $X(t)$ as simply the nearest grid point to the maximum, first-order convergence is expected (even though the numerical methods used to compute the solution are of higher order). Hence these results suggest that the computed solution has a constant shape, up to numerical error.

4.2. Speed-amplitude relation. There is a simple relationship between the x-momentum amplitude $A = \max_{x,y} \rho|u|$ of a diffracton and its speed, V. In order to demonstrate this, we take a very broad initial condition:

$$\sigma_0(x,y) = e^{-x^2/100}, \qquad u_0 = v_0 = 0. \tag{19}$$

The solution, which evolves into eight separate diffractons, is shown in Figure 5.

We isolate each diffracton and propagate it up to $t=100$ to measure its speed. The blue squares in Figure 6 (left) show the measured speeds versus the amplitude A. In addition, we show linear (solid red) and quadratic (dashed black) least-squares fitted curves (constrained to pass through the known value $V = c_{\text{eff}} = 1.25$ for zero-amplitude waves). It is clear that the speed-amplitude relation is nonlinear. In this respect, diffractons are different from stegotons, which appear to have a linear speed-amplitude relation [10]. Many other classes of solitary waves are known to have a nonlinear speed-amplitude relationship; see, for instance, [18, 1, 4].

We have found (empirically) the very simple relation $V \approx \frac{\max \sigma(x,y)}{A}$. Indeed, to high accuracy we observe that

$$V \approx \frac{\sigma}{\rho|u|}. \tag{20}$$

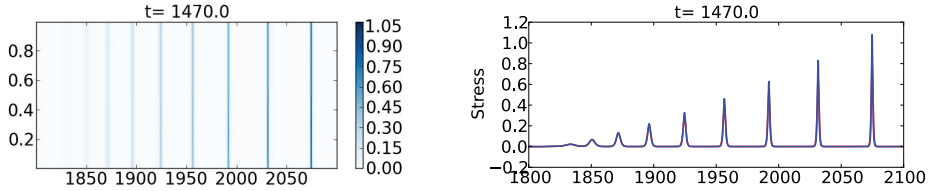

FIG. 5. *Train of diffractons used to study scaling properties and the speed-amplitude relation. Left: Stress as a function of x and y. Right: Slices at the middle of material A (blue) and B (red).*

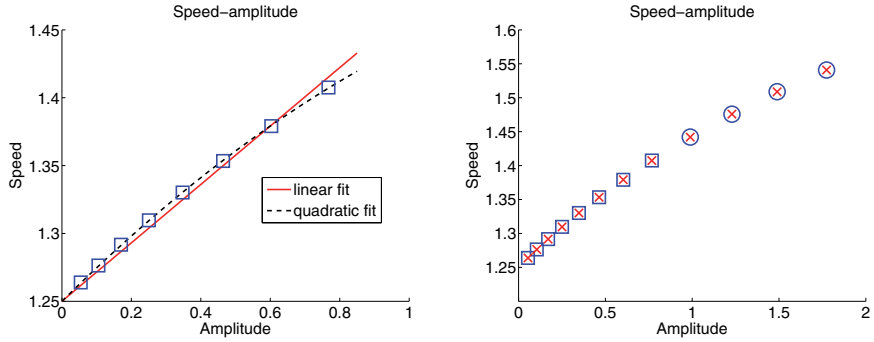

FIG. 6. *Speed-amplitude relationship for diffractons. The blue marks denote measurements. Left: Linear (solid red) and quadratic (dashed black) least-squares fits. Right: Comparison with values predicted by* (20) *(red crosses). The squares and circles are measurements made from the eight diffractons in Figure* 5 *and by a scaling procedure described in section* 4.3*, respectively.*

Here the numerator and denominator are functions of x and y, but the ratio is essentially constant whenever $|u|$ is much larger than roundoff. In Figure 6 (right) we show the speed predicted by (20) (red crosses) and the measured speed (blue squares) for the first eight diffractons in Figure 5 and for four larger diffractons obtained by a scaling procedure described in section 4.3 (blue circles). The values are indistinguishable.

In experiments with media obtained by other choices of $(K_A, K_B, \rho_A, \rho_B)$ we have found that the speed of each solitary wave is always given to high accuracy by the ratio $\max_x \sigma / \max_x(\rho|u|)$, and this value is independent of y. But for other media it is not always true that the value $\sigma/(\rho|u|)$ is the same for all x within a given solitary wave.

4.3. Scaling. Many one-dimensional solitary waves (such as the soliton solutions of the Korteweg–de Vries equation) are known to have a shape identical or similar to that of the function $sech^2(x)$; furthermore, the width of a solitary wave often varies inversely with the square root of its amplitude. These properties were found to hold approximately for stegotons in [10]. In this section we investigate the shape and scaling relations of diffractons. For each fixed value y_0, we study the one-dimensional cross-section

$$f_{y_0}(x) := f(x, y_0),$$

where f may stand for the stress σ or the x- or y-momentum $(\rho u, \rho v)$. We emphasize that the subscript here does not stand for differentiation.

We find that, for each fixed y_0, the one-dimensional cross-sections of the x-momentum of the diffractons have a roughly $sech^2$ shape, and their width scales

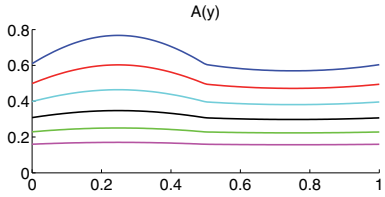

FIG. 7. *Maximum x-momentum as a function of y for each of the first six diffractons in Figure* 5.

inversely with the square root of the amplitude, although the amplitude of the cross-section is different for each y value.

Let $A(y)$ denote the maximum value of the x-momentum for a fixed y, and let $X(y)$ denote the location of the maximum:

$$A(y) = \max_x \rho(x,y)|u(x,y)|,$$
$$X(y) = \text{argmax}_x \rho(x,y)|u(x,y)|.$$

We find empirically that X is independent of y. The amplitude function for various diffractons is plotted in Figure 7. Then the stress and x-momentum of each cross-section of different diffractons appear to have the same shape under the transformation:

$$f_{y_0}(x) \to \frac{1}{A(y_0)} f\left(\sqrt{A(y_0)}(x - X)\right).$$

Of course, the transformed stress peak amplitudes of different waves are not equal since they are just the velocities of the corresponding diffractons; see (20). In Figures 8(a) and 8(b), we have plotted these transformed values for the leading six diffractons from Figure 5 along the line $y_0 = 1/8$. Slices at other y-values look similar. In Figure 8(b) we have also plotted (dashed line) a $sech^2$ function with amplitude and width fitted to the data.

Figure 8(c) shows the values of ρv under the same transformation. The locations of the extrema of the different curves coincide, but the amplitudes do not. We have also plotted (dashed line) the function $\partial_x\, sech^2$, again with amplitude and width fitted to the data. Finally, in Figure 8(d), we plot the y-momentum under the empirically determined transformation

$$f_{y_0}(x) \to \frac{1}{A(y_0)^{1.4}} f\left(\sqrt{A(y_0)}(x - X)\right),$$

which seems to scale the amplitudes almost equally.

4.4. Interaction of diffractons. We now investigate the behavior of colliding diffractons. The diffractons used for these experiments are shown in the top-left panel of Figure 9. All plots shown are y-slices of the stress at the middle of material A (blue) and material B (red).

4.4.1. Copropagating collision. In this scenario, both waves are moving to the right. Figure 9 shows the stress at different times during the interaction (solid line). For comparison, the dashed line shows the propagation of the taller wave by itself. As in most solitary wave interactions, a clear phase shift is exhibited. No oscillations are visible after the interaction, as shown in the lower-right panel. This suggests that the interaction is elastic, which is often the case in copropagating collisions of solitons and other solitary waves [5, 20, 19].

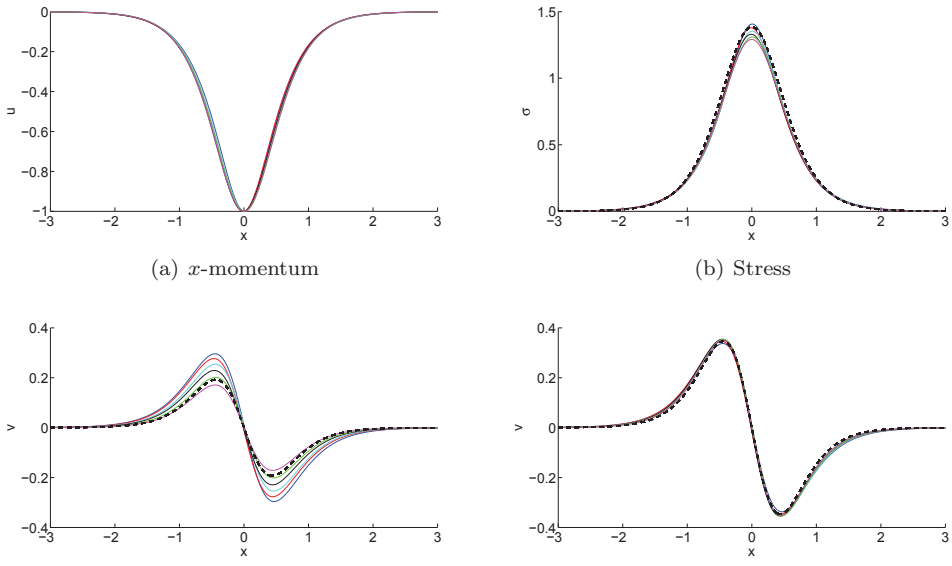

(a) x-momentum (b) Stress

(c) y-momentum (d) y-momentum, alternative scaling

FIG. 8. *Slices at $y = 1/8$ of rescaled velocities and stress. The dashed lines represent a sech^2 curve* (b) *and its derivative* (c)–(d).

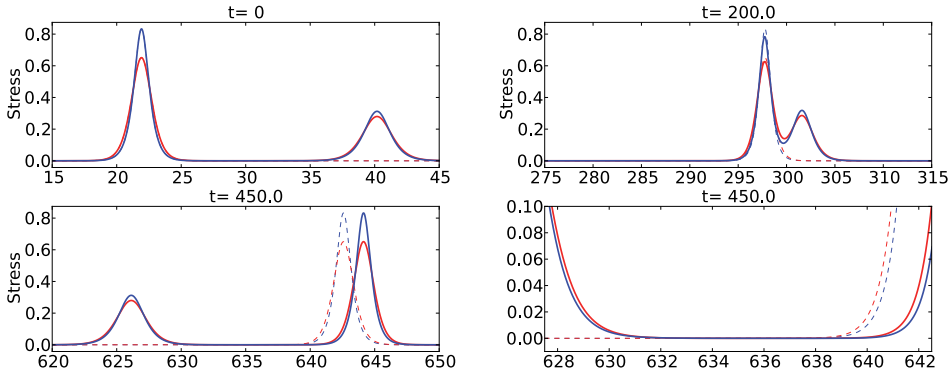

FIG. 9. *Copropagating collision at different times and a close-up of the tail of the diffractons after the interaction (bottom right). We show slices at the middle of materials A (blue) and B (red). The dashed lines represent the largest solitary wave propagating by itself, i.e., without collision.*

4.4.2. Counterpropagating collision. In Figure 10 we consider the same solitary waves in the same initial locations, but we negate the velocity fields u, v of the shorter wave to make it propagate to the left while the taller wave propagates to the right. This time there is barely a trace of phase shift; this is typical when the interaction time is so short. Oscillations *are* seen after the collision.

To investigate whether the oscillations are numerical or physical, in Figure 11 we repeat the same simulation on a grid with half as many points using SharpClaw and on the same grid using Clawpack with a TVD slope-limiter. Essentially no change in the solution is observed, strongly suggesting that the oscillations are physical (i.e., the counterpropagating collision is not elastic). This behavior has been observed for

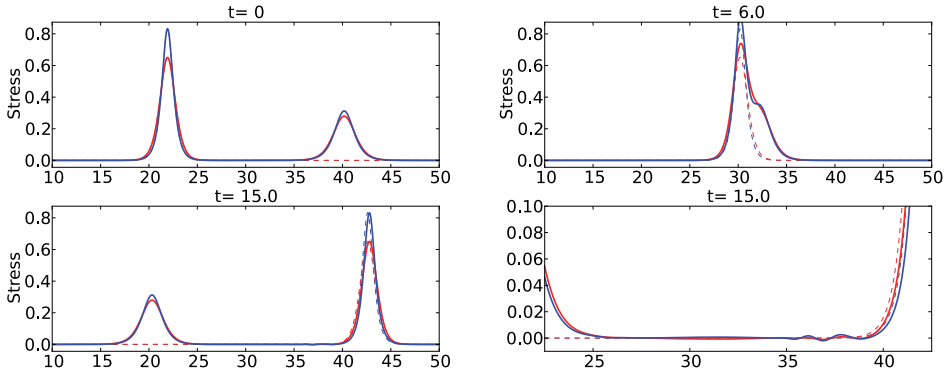

FIG. 10. *Counterpropagating collision at different times and a close-up of the tail of the diffractons after the interaction (bottom right). We show slices at the middle of materials A (blue) and B (red). The dashed lines represent the largest solitary wave propagating by itself, i.e., without collision.*

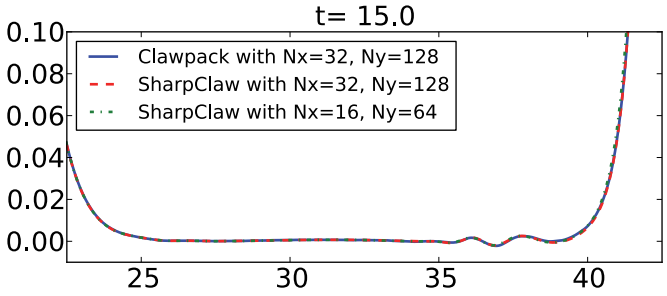

FIG. 11. *Close-up of the tail of the diffractons after a counterpropagating collision using Clawpack on a grid with $N_x = 32$ and $N_y = 128$ grid points per unit in x and y, respectively (solid blue line), SharpClaw on the same grid (dashed red line), and SharpClaw on a coarser grid with $N_x = 16$ and $N_y = 64$ (dotted green line). In this case, just the y-slice at the middle of material A is shown.*

other solitary waves, e.g., in [15, 11, 3].

5. Generalizations. The formation of solitary waves in general results from a balance between dispersion and nonlinearity. This section demonstrates that diffracton solutions exist under a broad range of scenarios.

5.1. Smoothly varying medium. Effective dispersion due to diffraction occurs not only in the piecewise-constant media we have focused on but also more generally in any periodic medium with variable sound speed. As an example, we consider a sinusoidally varying medium, with coefficients

$$K(y) = \frac{K_A + K_B}{2} + \frac{K_A - K_B}{2} \sin(2\pi y), \tag{21a}$$

$$\rho(y) = \frac{1}{K(y)}. \tag{21b}$$

We solve the homogenized equations (11) for a transverse perturbation. We take the material parameters (7) and as initial data the Gaussian stress perturbation (12). The coefficients in this case are different from those for the piecewise medium; see

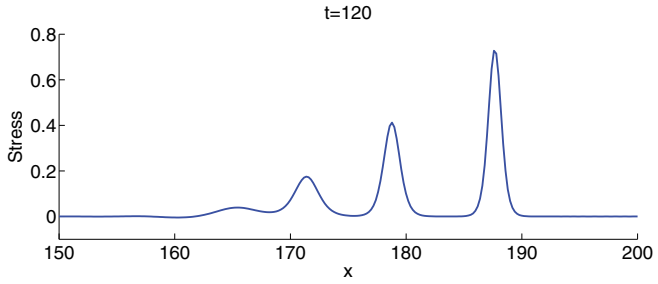

FIG. 12. *Homogenized diffractons for a sinusoidal medium given by* (21).

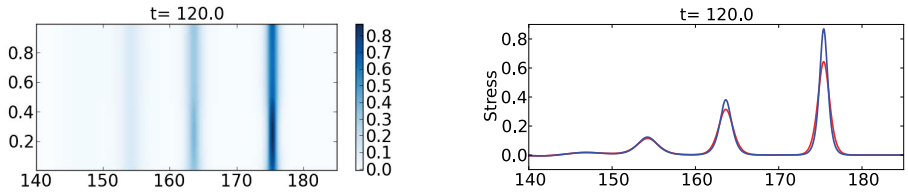

FIG. 13. *Diffracton solutions of* (1) *with the quadratic nonlinearity* (22). *Left: Surface plot of the stress at* $t = 120$. *Right: Slices at the middle of material A (blue) and material B (red).*

Appendix C. Figure 12 shows the solution at $t = 120$; solitary wave solutions are again observed.

5.2. Quadratic nonlinearity. By the same token, diffractons may arise in the presence of quite general nonlinearities—not just the exponential relation we have used. As an example, Figure 13 shows the solution of (1) obtained with the stress relation

$$\sigma = K(x)\epsilon + K(x)^2\epsilon^2, \tag{22}$$

with initial condition (12), where K, ρ are given by (7).

5.3. Wave propagation under reflection and diffraction. Waves that travel obliquely through a periodic medium like those considered here undergo both reflection (if the impedance varies) and diffraction (if the sound speed varies). Thus, in general they experience two types of effective dispersion [10, 13]. Figure 14 shows three experiments demonstrating the possible scenarios. For all three cases, the initial velocities are zero, and the initial stress (shown in Figure 14(a)) is

$$\sigma(x, y, t = 0) = 5\exp(-(x^2 + y^2)/10). \tag{23}$$

We show only the upper-right quadrant since the solution is symmetric.

In Figure 14(b), we take the material parameters (6), with the impedance mismatched and the sound speed matched. This generates dispersion by reflections. In this case, the solution develops a shock in the x-direction and solitary waves in the y-direction. In Figure 14(c), we use material parameters (7) with the impedance matched and the sound speed mismatched. This introduces dispersion by diffraction. As a result, the wave develops a shock in the y-direction and solitary waves in the x-direction. Finally, in Figure 14(d), we consider a medium with $K_A = 16$ and $\rho_A = K_B = \rho_B = 1$, which leads to $Z_A = 4$, $Z_B = 1$, $c_A = 4$, and $c_B = 1$; i.e., the

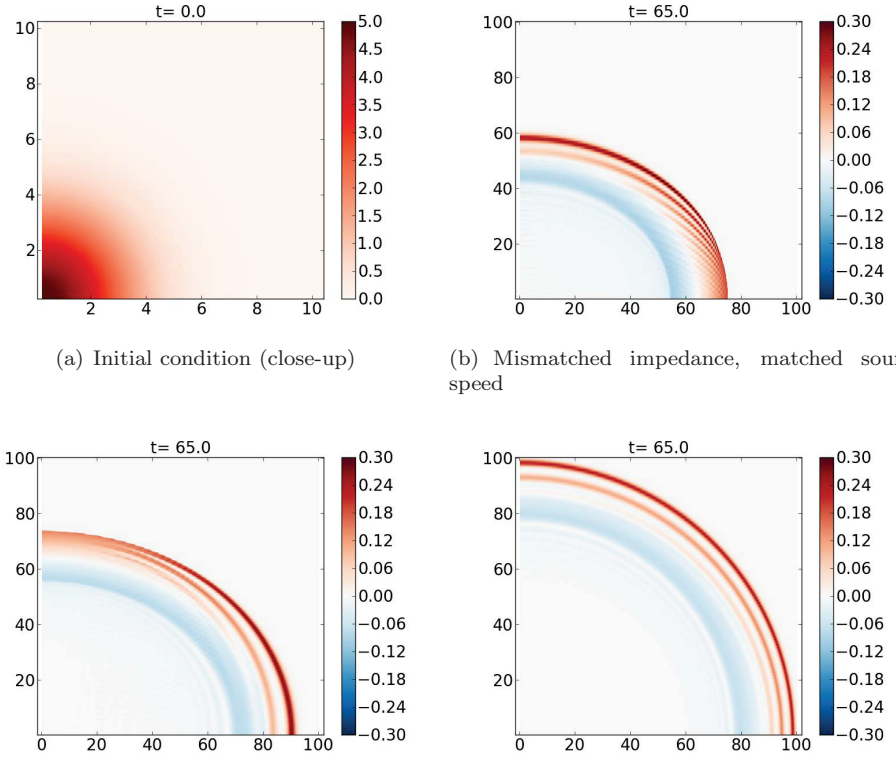

(a) Initial condition (close-up)

(b) Mismatched impedance, matched sound speed

(c) Matched impedance, mismatched sound speed

(d) Mismatched impedance and sound speed

FIG. 14. *Stress at $t = 0$ and $t = 65$ in different media.*

impedance and the sound speed are both mismatched. Effective dispersion due to reflections is introduced for waves traveling parallel to the y-axis due to diffraction for waves traveling parallel to the x-axis and a combination of both dispersion and diffraction if the wave travels in any other direction. A solitary wave develops that is almost cylindrically symmetric.

6. Conclusions and future work. We have seen that typical solutions of the model (1) involve solitary wave trains and that the effective dispersion responsible for these waves is an effect of small-scale diffraction. Intuitively, it seems that diffraction, like reflection, leads to dispersion through interference of high-frequency wave components. We are currently investigating the appearance of diffractive solitary waves in other physical wave models.

For large enough initial data, solutions of (1) may involve shock waves. These shock waves can turn into solitary waves after shedding a sufficient amount of energy. Investigation of shock wave formation and propagation in one- and two-dimensional periodic media is ongoing.

The homogenized equations derived in this work contain nonlinear dispersive terms. In some cases, similar terms in other equations have been shown to lead to ill-posedness [2]. We have not observed any behavior suggesting ill-posedness in our pseudospectral simulations or in simulations of the homogenized equations for

one-dimensional periodic media derived in [10]. Investigation of the well-posedness of these equations is beyond the scope of the present work.

Appendix A. Numerical methods. Solutions of the variable-coefficient system (1) in this work are computed using PyClaw [8, 16]. The algorithm used is referred to as SharpClaw and is based on a WENO discretization in space and a strong stability preserving (SSP) Runge–Kutta method in time [9]. For the Riemann solvers used and accuracy tests, see [12].

To solve the homogenized equations we use a pseudospectral spatial discretization from [17] with a fourth-order Runge–Kutta method in time.

All code used to generate the results in this work is available at https://www.github.com/ketch/diffractons_RR.git.

Appendix B. Derivation of homogenized equations. The homogenized equations presented in section 3 are derived through a nonlinear extension of the work in [13] applied to system (3) with the constitutive relation (2). Here we work through the derivation; the reader is referred to [13] for even more detail.

Using (2), we can write $\sigma_\epsilon = K(y)\,G(\sigma)$, where $G(\sigma) = \sigma + 1$. Using the chain rule, we have $\sigma_t = \sigma_\epsilon \epsilon_t$; we transform (3) into

$$K^{-1}(y)\,\sigma_t - G(\sigma)\,(u_x + v_y) = 0, \tag{24a}$$

$$\rho(y)\,u_t - \sigma_x = 0, \tag{24b}$$

$$\rho(y)\,v_t - \sigma_y = 0. \tag{24c}$$

Next we introduce the small parameter δ explained in section 3 and the fast scale $\hat{y} = \delta^{-1} y$. By the chain rule, $\partial_y \mapsto \partial_y + \delta^{-1}\partial_{\hat{y}}$. Using the formal expansion $\sigma(x, y, \hat{y}, t) = \sum_{i=0}^{\infty} \delta^i \sigma_i(x, y, \hat{y}, t)$ and similarly for u and v, we get

$$K^{-1}\sum_{i=0}^{\infty}\delta^i\sigma_{i,t} - G(\sigma)\left(\sum_{i=0}^{\infty}\delta^i u_{i,x} + \sum_{i=0}^{\infty}\delta^i v_{i,y} + \delta^{-1}\sum_{i=0}^{\infty}\delta^i v_{i,\hat{y}}\right) = 0, \tag{25a}$$

$$\rho\sum_{i=0}^{\infty}\delta^i u_{i,t} - \sum_{i=0}^{\infty}\delta^i\sigma_{i,x} = 0, \tag{25b}$$

$$\rho\sum_{i=0}^{\infty}\delta^i v_{i,t} - \left(\sum_{i=0}^{\infty}\delta^i\sigma_{i,y} + \delta^{-1}\sum_{i=0}^{\infty}\delta^i\sigma_{i,\hat{y}}\right) = 0, \tag{25c}$$

where $(\cdot)_{i,x}$ denotes differentiation of $(\cdot)_i$ with respect to x. The function $G(\sigma)$ is expanded around σ_0 using Taylor series as $G(\sigma) = G(\sigma_0) + \delta\sigma_1 + \delta^2\sigma_2 + \ldots$, where we use the fact that $G'(\sigma) = 1$ and all higher derivatives of G vanish.

Next we equate terms of the same order in (25). At each order we apply the averaging operator $\langle\cdot\rangle := \int_{\mathcal{C}}(\cdot)\,d\hat{y}$ (where $\mathcal{C}$ denotes the unit cell of the medium) to obtain the homogenized leading-order system and corrections to it. At each order, we make an ansatz to obtain an expression for the nonhomogenized solution.

B.1. Derivation of the homogenized $\mathcal{O}(1)$ system. Equating $\mathcal{O}\left(\delta^{-1}\right)$ terms in (25) and noting that $G(\sigma_0) \neq 0$, we conclude that $v_0 = v_0(x, y, t) =: \bar{v}_0(x, y, t)$ and $\sigma_0 = \sigma_0(x, y, t) =: \bar{\sigma}_0(x, y, t)$ (the bar denotes variables that are independent of the fast scale $\hat{y}$). We cannot conclude that u_0 is independent of the fast scale $\hat{y}$; indeed,

we will soon see that it is not. Now take the $\mathcal{O}(1)$ terms in (25) to get

$$K^{-1}\bar{\sigma}_{0,t} - G(\bar{\sigma}_0)(u_{0,x} + \bar{v}_{0,y} + v_{1,\hat{y}}) = 0, \tag{26a}$$

$$\rho u_{0,t} - \bar{\sigma}_{0,x} = 0, \tag{26b}$$

$$\rho \bar{v}_{0,t} - \bar{\sigma}_{0,y} - \sigma_{1,\hat{y}} = 0. \tag{26c}$$

Divide the second equation by ρ and apply the average operator $\langle\cdot\rangle$ to get

$$K_h^{-1}\bar{\sigma}_{0,t} - G(\bar{\sigma}_0)(\bar{u}_{0,x} + \bar{v}_{0,y}) = 0, \tag{27a}$$

$$\rho_h \bar{u}_{0,t} - \bar{\sigma}_{0,x} = 0, \tag{27b}$$

$$\rho_m \bar{v}_{0,t} - \bar{\sigma}_{0,y} = 0, \tag{27c}$$

where (based on periodicity) we have used $\langle v_{1,\hat{y}}\rangle = \langle\sigma_{1,\hat{y}}\rangle = 0$. Equation (27) is the homogenized leading-order system. It has the same form as (24), but with constant coefficients.

From (26b) and (27b), using an appropriate initial condition for $\bar{u}_0$, one obtains the following relation between u_0 and $\bar{u}_0$:

$$u_0 = \frac{\rho_h}{\rho(\hat{y})}\bar{u}_0. \tag{28}$$

This confirms that u_0 varies on the fast scale $\hat{y}$. Importantly, this shows that propagation in x and the heterogeneity in y are coupled even at the macroscopic scale.

We now find an expression for the nonaveraged $\mathcal{O}(1)$ terms in (26). To do so, we make the following ansatz:

$$v_1 = \bar{v}_1 + A(\hat{y})\,\bar{u}_{0,x} + B(\hat{y})\,\bar{v}_{0,y}, \tag{29a}$$

$$\sigma_1 = \bar{\sigma}_1 + C(\hat{y})\,\bar{\sigma}_{0,y}. \tag{29b}$$

This ansatz is chosen in order to reduce system (26) to a system of ODEs. Substituting the ansatz (29), the relation for u_0 (28), and the homogenized leading-order system (27) into the $\mathcal{O}(1)$ system (26) and requiring that the fast variable coefficients vanish, we get

$$A_{\hat{y}} = K^{-1}K_h - \rho^{-1}\rho_h, \tag{30a}$$

$$B_{\hat{y}} = K^{-1}K_h - 1, \tag{30b}$$

$$C_{\hat{y}} = \rho\rho_m^{-1} - 1, \tag{30c}$$

with the normalization conditions that $\langle A\rangle = \langle B\rangle = \langle C\rangle = 0$. Note that $\langle A_{\hat{y}}\rangle = \langle B_{\hat{y}}\rangle = \langle C_{\hat{y}}\rangle = 0$, which implies that A, B, and C are periodic.

B.2. Derivation of the homogenized $\mathcal{O}(\delta)$ system. From (25) take terms of order $\mathcal{O}(\delta)$:

$$K^{-1}\sigma_{1,t} - G(\bar{\sigma}_0)(u_{1,x} + v_{1,y} + v_{2,\hat{y}}) - \sigma_1(u_{0,x} + \bar{v}_{0,y} + v_{1,\hat{y}}) = 0, \tag{31a}$$

$$\rho u_{1,t} - \sigma_{1,x} = 0, \tag{31b}$$

$$\rho v_{1,t} - \sigma_{1,y} - \sigma_{2,\hat{y}} = 0. \tag{31c}$$

Plug the ansatz for u_1, v_1, and σ_1 from (29) into (31) and take the average $\langle\cdot\rangle$ to

get

$$\begin{aligned} K_h^{-1}\bar{\sigma}_{1,t} - G\left(\bar{\sigma}_0\right)\left(\bar{u}_{1,x}+\bar{v}_{1,y}\right) - \bar{\sigma}_1\left(\bar{u}_{0,x}+\bar{v}_{0,y}\right) &= -\left\langle K^{-1}C\right\rangle \bar{\sigma}_{0,yt} + \left\langle CB_{\hat{y}}\right\rangle \bar{\sigma}_{0,y}\bar{v}_{0,y} \\ &\quad + \left(\rho_h\left\langle \rho^{-1}C\right\rangle + \left\langle CA_{\hat{y}}\right\rangle\right)\bar{\sigma}_{0,y}\bar{u}_{0,x}, \\ \rho_h\bar{u}_{1,t} - \bar{\sigma}_{1,x} &= \rho_h\left\langle \rho^{-1}C\right\rangle \bar{\sigma}_{0,xy}, \\ \rho_m\bar{v}_{1,t} - \bar{\sigma}_{1,y} &= -\left\langle \rho \mathrm{A}\right\rangle \bar{u}_{0,xt} - \left\langle \rho B\right\rangle \bar{v}_{0,yt}. \end{aligned}$$

For many materials, including the layered and sinusoidal media considered in this work, it is true that $\left\langle K^{-1}C\right\rangle = \left\langle \rho^{-1}C\right\rangle = \left\langle CA_{\hat{y}}\right\rangle = \left\langle CB_{\hat{y}}\right\rangle = \left\langle \rho^{-1}C\right\rangle = \left\langle \rho A\right\rangle = \left\langle \rho B\right\rangle = 0$. Therefore, we obtain

$$K_h^{-1}\bar{\sigma}_{1,t} - G\left(\bar{\sigma}_0\right)\left(\bar{u}_{1,x}+\bar{v}_{1,y}\right) - \bar{\sigma}_1\left(\bar{u}_{0,x}+\bar{v}_{0,y}\right) = 0, \tag{32a}$$

$$\rho_h\bar{u}_{1,t} - \bar{\sigma}_{1,x} = 0, \tag{32b}$$

$$\rho_m\bar{v}_{1,t} - \bar{\sigma}_{1,y} = 0. \tag{32c}$$

Since the boundary conditions are imposed in the leading-order homogenized system, system (32) has zero boundary conditions and no forcing terms; therefore, its solution vanishes:

$$\bar{u}_1 = \bar{v}_1 = \bar{\sigma} = 0.$$

We now make an ansatz for the nonaveraged $\mathcal{O}(\delta)$ terms v_2 and σ_2 in system (31):

$$v_2 = \bar{v}_2 + D(\hat{y})\bar{u}_{0,xy} + E(\hat{y})\bar{v}_{0,yy}, \tag{33a}$$

$$\sigma_2 = \bar{\sigma}_2 + F(\hat{y})\bar{\sigma}_{0,yy} + H(\hat{y})\bar{\sigma}_{0,xx}. \tag{33b}$$

From (31b) we have $u_{1,t} = \rho^{-1}\sigma_{1,x}$. Then use the ansatz for σ_1 from (29b) to get $u_{1,t} = \rho^{-1}C(\bar{\sigma}_{0,x})_y$ and the homogenized leading-order equation (27b) to get $u_{1,t} = \rho^{-1}\rho_h C(\bar{u}_{0,y})_t$. Finally, using an appropriate initial condition for $\bar{u}_0$, we get an expression for the nonaveraged solution u_1:

$$u_1 = \rho^{-1}\rho_h C\bar{u}_{0,y}. \tag{34}$$

Substitute the ansatz (29) for v_1 and σ_1, the ansatz (33) for v_2 and σ_2, the nonhomogenized solution u_1 (34), the leading-order homogenized system (27), and the ODEs (30) for A, B, and C into (31) and set the fast variable coefficients to zero to get

$$\begin{aligned} D_{\hat{y}} &= K^{-1}K_hC - \rho^{-1}\rho_hC - A, \\ E_{\hat{y}} &= K^{-1}K_hC - B, \\ F_{\hat{y}} &= \rho\rho_m^{-1}B - C, \\ H_{\hat{y}} &= \rho\rho_h^{-1}A, \end{aligned}$$

with the normalization condition $\langle D\rangle = \langle E\rangle = \langle F\rangle = \langle H\rangle = 0$. Again note that $\langle D_{\hat{y}}\rangle = \langle E_{\hat{y}}\rangle = \langle F_{\hat{y}}\rangle = \langle H_{\hat{y}}\rangle = 0$, which implies that D, E, F, and H are periodic.

B.3. Derivation of the homogenized $\mathcal{O}(\delta^2)$ system. From (25) take $\mathcal{O}(\delta^2)$ terms:

$$K^{-1}\sigma_{2,t} - G(\bar{\sigma}_0)(u_{2,x}+v_{2,y}+v_{3,\hat{y}}) - \sigma_1(u_{1,x}+v_{1,y}+v_{2,\hat{y}}) - \sigma_2(u_{0,x}+\bar{v}_{0,y}+v_{1,\hat{y}}) = 0, \tag{35a}$$

$$\rho u_{2,t} - \sigma_{2,x} = 0, \tag{35b}$$

$$\rho v_{2,t} - \sigma_{2,y} - \sigma_{3,\hat{y}} = 0. \tag{35c}$$

Plug the ansatz for u_1, v_1, and σ_1 from (29) and the ansatz for u_2, v_2, and σ_2 from (33) into (35) and take the average $\langle\cdot\rangle$ to get

$$\begin{aligned}
K_h^{-1}\bar{\sigma}_{2,t} - G\left(\bar{u}_{2,x} + \bar{v}_{2,y}\right) & \\
-\bar{\sigma}_2\left(\bar{u}_{0,x} + \bar{v}_{0,y}\right) &= -K_h\left\langle K^{-1}F\right\rangle\left[G\left(\bar{u}_{0,xyy} + \bar{v}_{0,yyy}\right) + 2\bar{\sigma}_{0,y}\left(\bar{u}_{0,xy} + \bar{v}_{0,yy}\right)\right] \\
&\quad - K_h\left\langle K^{-1}H\right\rangle\left[G\left(\bar{u}_{0,xxx} + \bar{v}_{0,xxy}\right) + 2\bar{\sigma}_{0,x}\left(\bar{u}_{0,xx} + \bar{v}_{0,xy}\right)\right] \\
&\quad + K_h\left\langle K^{-1}C^2\right\rangle\bar{\sigma}_{0,y}\left(\bar{u}_{0,xy} + \bar{v}_{0,yy}\right), \qquad \text{(36a)} \\
\rho_h\bar{u}_{2,t} - \bar{\sigma}_{2,x} &= \rho_h\left\langle\rho^{-1}F\right\rangle\bar{\sigma}_{0,xyy} + \rho_h\left\langle\rho^{-1}H\right\rangle\bar{\sigma}_{0,xxx}, \qquad \text{(36b)} \\
\rho_m\bar{v}_{2,t} - \bar{\sigma}_{2,y} &= -\rho_h^{-1}\left\langle\rho D\right\rangle\bar{\sigma}_{0,xxy} - \rho_m^{-1}\left\langle\rho E\right\rangle\bar{\sigma}_{0,yyy}. \qquad \text{(36c)}
\end{aligned}$$

B.4. Combine homogenized leading order and corrections. Once we have the homogenized leading-order system and the homogenized corrections, we combine them into a single system, using the relation $\sigma := \langle\sigma_0 + \delta\sigma_1 + \dots\rangle$, and similarly for u and v. Combining homogenized systems (27), (32), and (36), we obtain

$$\begin{aligned}
K_h^{-1}\sigma_t - (\sigma+1)\left(u_x + v_y\right) &= \delta^2\alpha_1\left[(\sigma+1)\left(u_{xyy} + v_{yyy}\right) + 2\sigma_y\left(u_{xy} + v_{yy}\right)\right] \\
&\quad + \delta^2\alpha_2\left[(\sigma+1)\left(u_{xxx} + v_{xxy}\right) + 2\sigma_x\left(u_{xx} + v_{xy}\right)\right] \\
&\quad + \delta^2\alpha_3\sigma_y\left(u_{xy} + v_{yy}\right), \\
\rho_h u_t - \sigma_x &= \delta^2\beta_1\sigma_{xyy} + \delta^2\beta_2\sigma_{xxx}, \\
\rho_m v_t - \sigma_y &= \delta^2\gamma_1\sigma_{yyy} + \delta^2\gamma_2\sigma_{xxy},
\end{aligned}$$

where

$$\begin{aligned}
&\alpha_1 = -K_h\left\langle K^{-1}F\right\rangle, && \alpha_2 = -K_h\left\langle K^{-1}H\right\rangle, && \alpha_3 = K_h\left\langle K^{-1}C^2\right\rangle, \\
&\beta_1 = \rho_h\left\langle\rho^{-1}F\right\rangle, && \beta_2 = \rho_h\left\langle\rho^{-1}H\right\rangle, && \\
&\gamma_1 = -\rho_m^{-1}\left\langle\rho E\right\rangle, && \gamma_2 = -\rho_h^{-1}\left\langle\rho D\right\rangle. &&
\end{aligned}$$

Formulas for these coefficients in the case of a piecewise-constant medium are given by (9).

Appendix C. Coefficients of the homogenized equations on sinusoidal medium. In this appendix we compute the coefficients of the homogenized equation (11), which considers waves traveling transversally (to the heterogeneity).

For the sinusoidal medium and for more general y-periodic media, it is difficult to find closed expressions for the fast-variable functions and for the coefficients. Therefore, we solve the boundary value problems and compute the coefficients numerically. Details can be found at https://www.github.com/ketch/diffractons_RR.git. The files available can easily be modified to produce coefficients for other media. The numerically computed coefficients are

$$\begin{aligned}
\alpha_2 &= 0.013208894074369, \\
\beta_2 &= 0.011033010870322.
\end{aligned}$$

REFERENCES

[1] B.F. Akers, *Model Equations for Gravity-Capillary Waves*, Ph.D. thesis, The University of Wisconsin-Madison, Madison, WI, 2008.

[2] D.M. Ambrose, G. Simpson, J.D. Wright, and D.G. Yang, *Ill-posedness of degenerate dispersive equations*, Nonlinearity, 25 (2012), pp. 2655–2680.

[3] J.G.B. Byatt-Smith, *The head-on interaction of two solitary waves of unequal amplitude*, J. Fluid Mech., 205 (1989), pp. 573–579.

[4] A. Duran, D. Dutykh, and D. Mitsotakis, *On the Galilean invariance of some nonlinear dispersive wave equations*, Stud. Appl. Math., 131 (2013), pp. 359–388.

[5] R. Hirota, *Exact solution of the Korteweg-de Vries equation for multiple collisions of solitons*, Phys. Rev. Lett., 27 (1971), pp. 1192–1194.

[6] D.I. Ketcheson, *High Order Strong Stability Preserving Time Integrators and Numerical Wave Propagation Methods for Hyperbolic PDEs*, Ph.D. thesis, University of Washington, Citeseer, 2009.

[7] D.I. Ketcheson and R.J. LeVeque, *Shock dynamics in layered periodic media*, Commun. Math. Sci., 10 (2012), pp. 859–874.

[8] D.I. Ketcheson, K.T. Mandli, A.J. Ahmadia, A. Alghamdi, M. Quezada de Luna, M. Parsani, M.G. Knepley, and M. Emmett, *PyClaw: Accessible, extensible, scalable tools for wave propagation problems*, SIAM J. Sci. Comput., 34 (2012), pp. C210–C231.

[9] D.I. Ketcheson, M. Parsani, and R.J. LeVeque, *High-order wave propagation algorithms for hyperbolic systems*, SIAM J. Sci. Comput., 35 (2013), pp. A351–A377.

[10] R.J. LeVeque and D.H. Yong, *Solitary waves in layered nonlinear media*, SIAM J. Appl. Math., 63 (2003), pp. 1539–1560.

[11] R.M. Mirie and C.H. Su, *Collisions between two solitary waves. Part* 2. *A numerical study*, J. Fluid Mech., 115 (1982), pp. 475–492.

[12] M. Quezada de Luna and D.I. Ketcheson, *Numerical simulation of cylindrical solitary waves in periodic media*, J. Sci. Comput., 58 (2014), pp. 672–689.

[13] M. Quezada de Luna and D.I. Ketcheson, *Two-dimensional wave propagation in layered periodic media*, http://arxiv.org/abs/1309.6666, 2013.

[14] F. Santosa and W.W. Symes, *A dispersive effective medium for wave propagation in periodic composites*, SIAM J. Appl. Math., 51 (1991), pp. 984–1005.

[15] C.H. Su and R.M. Mirie, *On head-on collisions between two solitary waves*, J. Fluid Mech., 98 (1980), pp. 509–525.

[16] Clawpack Development Team, *Clawpack software*, Version 5.0, 2013.

[17] L.N. Trefethen, *Spectral Methods in MATLAB*, SIAM, Philadelphia, 2000.

[18] V. Vlasenko, P. Brandt, and A. Rubino, *Structure of large-amplitude internal solitary waves*, J. Physical Oceanography, 30 (2000), pp. 2172–2185.

[19] T. Yaotsu Wu, *Nonlinear waves and solitons in water*, Phys. D, 123 (1998), pp. 48–63.

[20] N.J. Zabusky and M.D. Kruskal, *Interaction of "solitons" in a collisionless plasma and the recurrence of initial states*, Phys. Rev. Lett., 15 (1965), pp. 240–243.